ACS APPLIED MATERIALS & INTERFACES

Subscriber access provided by UNIV OF NEW ENGLAND ARMIDALE

Biological and Medical Applications of Materials and Interfaces

Biodegradable Quantum Composites for Synergistic Photothermal Therapy and Copper-enhanced Chemotherapy

Han-Xiao Tang, Chen-Guang Liu, Jian-Ting Zhang, XIANG ZHENG, Da-Yun Yang, Ranjith Kumar Kankala, Shi-Bin Wang, and Ai-Zheng Chen

ACS Appl. Mater. Interfaces, **Just Accepted Manuscript** • DOI: 10.1021/acsami.0c14636 • Publication Date (Web): 25 Sep 2020

Biodegradable Quantum Composites for Synergistic Photothermal Therapy and Copper-enhanced Chemotherapy

*Han-Xiao Tang[a,b], Chen-Guang Liu[a,b], Jian-Ting Zhang[a,b], Xiang Zheng[a,b], Da-Yun Yang[c], Ranjith Kumar Kankala[a,b], Shi-Bin Wang[a,b], and Ai-Zheng Chen[a,b,]**

[a] Institute of Biomaterials and Tissue Engineering, Huaqiao University, Xiamen 361021, P.R. China

[b] Fujian Provincial Key Laboratory of Biochemical Technology (Huaqiao University), Xiamen 361021, P. R. China

[c] Institute for Translational Medicine, School of Basic Medical Sciences, Fujian Medical University, Fuzhou 350108, P. R. China

ABSTRACT

In recent times, the combination therapy has garnered enormous interest owing to its great potential in clinical research. It has been reported that disulfiram (DSF), a clinical anti-alcoholism drug, could be degraded to diethyldithiocarbamate (DDTC) *in vivo* and subsequently resulting in the copper-DDTC complex ($Cu(DDTC)_2$) towards ablating cancer cells. In addition, the ultra-small copper sulfide nanodots (CuS NDs) have shown great potential in cancer treatment because of their excellent photothermal and photodynamic therapeutic efficiency. Herein, by taking advantage of the interactions between CuS and DDTC, a new multi-functional nanoplatform, DDTC-loaded CuS (CuS-DDTC) NDs, is successfully fabricated, leading to the achievement of the synergistic effect of photothermal and copper enhanced chemotherapy. All experimental results verified promising synergistic therapeutic effects. Moreover, *in vivo* biocompatibility and metabolism experiments displayed that the CuS-DDTC NDs could be quickly excreted from the body with no apparent toxicity signs. Together, our findings indicated the superior synergistic therapeutic effect of photothermal and copper enhanced chemotherapy, providing a promising anti-cancer strategy based on CuS-DDTC NDs drug delivery system.

KEYWORDS Ultra-small copper sulfides nanodots; Disulfiram; Ion enhanced chemotherapy; Photothermal; Synergistic effect

INTRODUCTION

The combination of chemotherapy and photothermal therapy (PTT) has become a hot topic in clinical research due to the high selectivity and excellent therapeutic effect.[1-5] In this framework, various drug delivery systems (DDSs) based on inorganic or organic nanomaterials have been developed for efficient synergistic PTT and chemotherapy.[1, 5-8] However, several drawbacks still exist for current available therapeutic agents and DDSs, such as undesirable side effects, the potential toxicity of long-term retention *in vivo* and the unsatisfactory therapeutic efficiency, which greatly limit their clinical application.[9-13] Hence, it is urgent to develop new functional nanomaterials that can not only effectively cure cancer but also be cleared from the body to avoid retention toxicity[14].

Notably, the nanomaterials with a diameter smaller than 10 nm can be excreted quickly, avoiding retention toxicity. Therefore, DDSs based on nanodots have been attracted increased attention from researchers in recent years to avoid long-term toxicity by taking advantage of ultra-small sizes.[15-19] Moreover, by modifying polymers or functional groups on the surface, chemotherapeutic drugs such as doxorubicin can be conveniently loaded onto the nanodots for combined treatment.[15-18] However, current studies have been focused on the simple combination of PTT and chemotherapy, while the amplification and synergistic efficacy between photosensitizers and chemotherapeutic moieties are not carefully studied. Thus, the development of multi-functional nanodots DDSs for coordinated synergistic therapy is a promising approach to optimizing cancer therapy.[10, 20-22]

Recently, ultra-small copper sulfides nanodots (CuS NDs) have been widely used in combined therapy due to its excellent near-infrared (NIR) photothermal efficiency, good biodegradability,

inexpensive, and low toxicity.[23-25] Further, the CuS NDs can also release copper ions for reactive oxygen species (ROS) generation, towards photodynamic therapy (PDT). The released copper ions can also coordinate with specific prodrugs, exhibiting ultra-high anti-cancer efficiency.[26-27] In addition, CuS NDs have been used for photoacoustic (PA) imaging.[28-29]

Disulfiram (DSF), a clinical anti-alcoholism drug, has gained enormous interest in cancer therapy.[30-31] In recent years, DSF has been proved to be a copper-dependent anti-tumor drug.[26] After *in vivo* degradation of DSF, diethyldithiocarbamate (DDTC) is formed and subsequently complexed with copper ions, $Cu(DDTC)_2$, resulting in tumor apoptosis.[26] As the primary metabolite of DSF and an active substance for the formation of $Cu(DDTC)_2$, DDTC is applied for the enriched anti-cancer effect of DSF.[32-34] However, the limited supply of copper *in vivo* hampers the therapeutic ability of DSF. Therefore, the introduction of CuS NDs can be an effective way to solve the copper source issue. Owing to the intrinsic degradation and the stimulation by laser, the degraded CuS NDs deliver the copper ions and release them selectively at the tumor site. In addition, these CuS NDs can serve as ideal carriers and photothermal agents for coordinated synergistic therapy.

Based on these facts, we demonstrate the construction of a multi-functional nanoplatform on the basis of the complexation between DDTC and copper ions towards achieving the synergistic effect of photothermal and copper-enhanced chemotherapy through *in situ* chemical activation and photothermal enhancement. As shown in **Scheme 1**, DDTC was initially loaded on the surface of CuS NDs based on the complexation between copper ions and DDTC, resulting in CuS-DDTC NDs. $Cu(DDTC)_2$ would be generated after the complexation between copper and DDTC, resulting in enhanced chemotherapy efficacy. In this system, CuS NDs played four functions of photothermal agents for PTT, as DDSs to deliver drugs to the tumor site, as contrast agents for PA

and thermal imaging, and as a source of copper to increase the copper ion concentration at the tumor site and enhance the chemotherapeutic efficacy. In addition, the biocompatibility and metabolism of CuS NDs and CuS-DDTC NDs were evaluated *in vivo*. Finally, the multimodal imaging-guided synergistic therapy of CuS-DDTC NDs was systematically investigated.

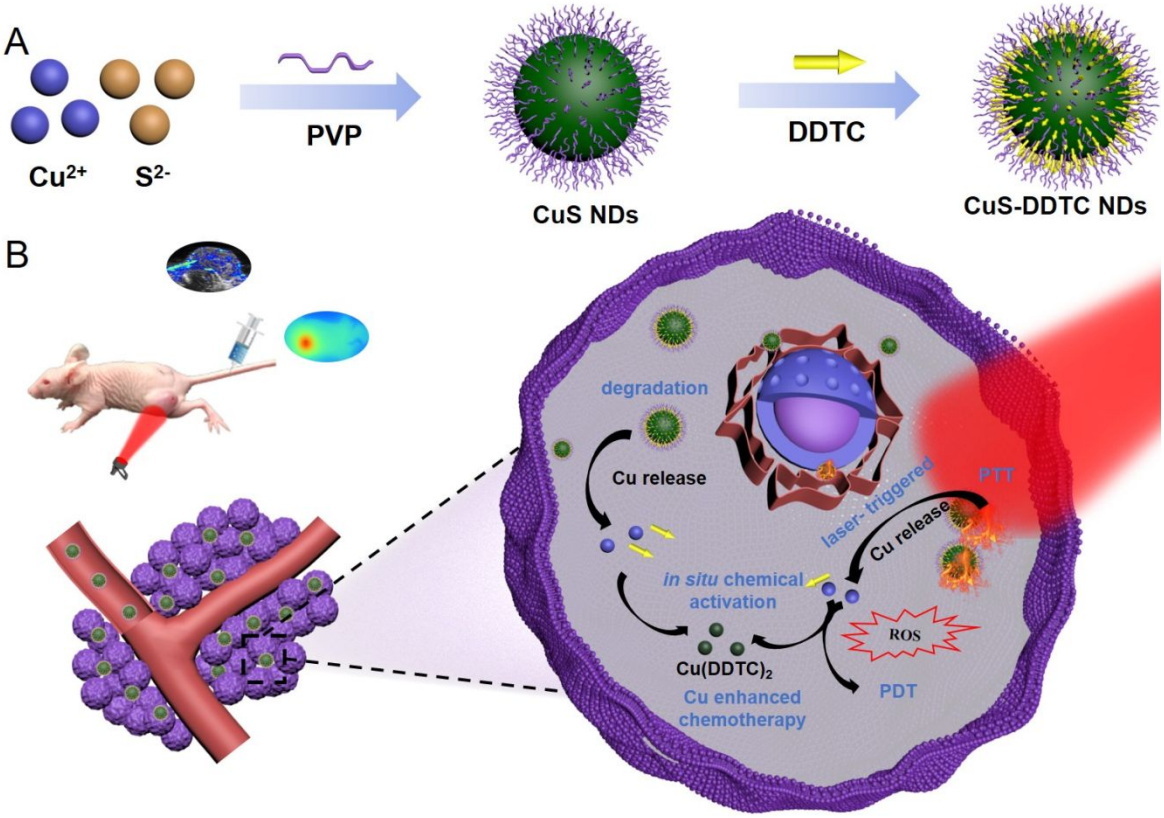

Scheme 1. Schematic illustration showing the (A) synthesis, and (B) photoacoustic imaging, as well as synergistic tumor therapy of CuS-DDTC NDs

MATERIALS AND METHODS

Materials. Sodium sulfide nonahydrate ($Na_2S{\cdot}9H_2O$), sodium diethyldithiocarbamate trihydrate (DDTC), phosphate-buffered saline (PBS), and copper chloride dihydrate ($CuCl_2{\cdot}2H_2O$) were obtained from Aladdin Reagent Co., Ltd. (Shanghai, China). Polyvinylpyrrolidone (PVP) K15

(viscosity average molecular 10,000 Da) was obtained from Tokyo Chemical Industry Co., Ltd. (Shanghai, China). Thiol-polyethylene glycol-fluorescein isothiocyanate (SH-PEG_{5000}-FITC) was obtained from Ruixi Biological Technology Co., Ltd. (Xian, China).

Synthesis of CuS NDs. CuS NDs were synthesized on the basis of the reported method.[25] Briefly, 17.05 mg of $CuCl_2 \cdot 2H_2O$ and 3 g of PVP K15 were added into water (100 mL), and the sample was heated to 90 °C under vigorous stirring. Then, Na_2S solution (0.1 mL, 1 M) was mixed and stirred for 20 min. Subsequently, the resultant CuS NDs were washed thrice and stored at 4 °C after lyophilization. FITC-labeled CuS NDs (FITC-CuS NDs) were prepared as follows: SH-PEG-FITC was reacted with a CuS NDs solution, the obtained sample was maintained for 3 h under stirring in the dark, then centrifuged and washed with ultrapure water thrice.

Synthesis of CuS-DDTC NDs. To prepare CuS-DDTC NDs, 1 mg of CuS NDs was stirred in DDTC solution for 20 min. Further, the CuS-DDTC NDs were collected and washed with ultrapure water to remove free DDTC. The DDTC content in CuS-DDTC NDs was determined by measuring the free DDTC content remained in the supernatant at 280 nm. Further, drug loading was calculated using the following equation:

$$\text{Drug loading (\%)} = \text{Weight}_{\text{DDTC loaded into the CuS NDs}} / \text{Weight}_{\text{CuS-DDTC NDs}} \times 100 \quad (1)$$

Characterizations. The morphological attributes of CuS NDs and CuS-DDTC NDs were analyzed by transmission electron microscopy (TEM, H-7650, Hitachi Limited, Tokyo, Japan). The zeta potential and hydrodynamic size were determined using dynamic light scattering (DLS, ZetaPALS, Malvern Instrument Ltd, UK) approaches. The average size of the NDs was analyzed by Nano Measurer 1.2 software (n = 200). Ultraviolet-visible-NIR (UV-vis-NIR) absorption spectra were obtained from the UV-vis-NIR spectrophotometer (UV-1800, Mapada, Shanghai,

China). The crystalline states of the nanodots were determined by X-ray diffraction (XRD, Smar/SmartLa, Rigaku, Tokyo, Japan).

***In vitro* photothermal and photodynamic efficacies.** CuS NDs aqueous solution (1 mL, 100 μg/mL) was exposed under an 808-nm laser for 15 min. The temperature was recorded by a thermocouple thermometer. Then, the photothermal conversion efficiencies (η) were analyzed using the following equation.[35]

$$\eta = \frac{hs(\Delta T_{max,\ mix} - \Delta T_{max,H_2O})}{I(1 - 10^{-A_{808}})} \quad (2)$$

Where I represent the laser power, s is the surface area of the container, A_{808} is the absorbance of the solution at 808 nm, h is the heat transfer coefficient, and ΔT is the temperature change.

Finally, the photothermal stability of CuS NDs was measured by cycle irradiation for 3 times. Meanwhile, the temperature change curves of CuS-DDTC NDs under the laser irradiation at 1.5 W/cm^2 were also examined. To detect the hydroxyl (•OH) generation, terephthalic acid (TA) was applied. Briefly, 50 μg of CuS NDs, TA (5 mM), and H_2O_2 (400 μM) were mixed in water (1 mL) and irradiated at 1.5 W/cm^2 for various times. The fluorescence of the TA solution under excitation at 360 nm was measured to detect the generation of •OH. To detect the singlet oxygen ($^1O_2$), 9,10-anthracenediyl-bis(methylene)dimalonic acid (ABMDMA) was employed. Briefly, 50 μg of CuS NDs, ABMDMA (100 μM), and H_2O_2 (400 μM) were mixed in water (1 mL) and irradiated at 1.5 W/cm^2 at various times. The generation of $^1O_2$ was detected by UV-vis-NIR spectra (380 nm). For the degradation study, CuS NDs (25 μg/mL) and CuS-DDTC NDs (25 μg/mL) were dispersed in PBS (2 mL, pH-7.4), and the degradation process at predetermined time points was analyzed by the UV-vis-NIR spectra.

Cellular internalization. Mouse breast cancer (4T1, Keygen, Nanjing, China) cells were seeded in 24-well plates (1×10^5 cells per well) and cultured with FITC-CuS NDs (30 μg/mL) at various times. Then, the 4T1 cells were stained with 4',6-diamidino-2-phenylindole (DAPI, Keygen). Finally, confocal laser scanning microscopy (CLSM, Leica TCS SP8, Braunschweig, Germany) was used to capture the images.

***In vitro* cytotoxicity.** To investigate the cytotoxicity of the nanodots, human umbilical vein endothelial cells (HUVECs, Keygen) and 4T1 cells were used. The cells were seeded in 96-well plates (5000 cells per well). Further, CuS NDs (100 μL) or CuS-DDTC NDs (100 μL) solution in Dulbecco's modified eagle medium (DMEM) were added and cultured for 24 h. The cell viabilities were then recorded using Cell Counting Kit-8 (CCK-8, Solarbio Co. Ltd, Beijing, China), along with DMEM as a control group. The cell viability was evaluated with the following equation:

$$\text{Cell viability (\%)} = OD_{sample} - OD_{blank} / OD_{control} - OD_{blank} \times 100 \quad (3)$$

For chemotherapy and photothermal therapy (chemo-PTT), after co-culture with CuS for 6 h, 4T1 cells were exposed under an 808-nm laser (1.5 W/cm^2, 5 min). Subsequently, the cell viabilities were determined. To observe live and dead cells, the cells were subjected to Acridine Orange/Ethidium Bromide (AO/EB, Solarbio) kit, and the fluorescent images were obtained with an inverted fluorescence microscope (Ci-L, Nikon, Tokyo, Japan).

Intracellular ROS generation *in vitro*. 4T1 cells were seeded in 24-well plates (1×10^5 cells per well) and cultured with CuS NDs or CuS-DDTC NDs for 6 h. Then, the 4T1 cells were exposed with/without 808 nm laser (1.5 W/cm^2, 5 min) and subsequently incubated for 3 h. Finally, 4T1 cells were dyed with 2,7-dichlorodihydrofluorescein diacetate (DCFH-DA, Keygen) for 2 h, and the ROS generation was analyzed by CLSM.

Tumor model. The animal experiments were carried out following the protocol approved by the Experimental Animal Ethics Committee of Fujian Medical University. 4T1 cells (5×10^6) were injected into the nude mice (Huafukang Bioscience Co. Ltd., Beijing, China) in the right hind limbs to establish the tumor model. When the tumor volumes were increased to around 100 mm^3, the 4T1 tumor-bearing mice (4T1-TBM) were used for *in vivo* investigations.

PA imaging. PA imaging was measured using a PA imaging system (Endra Nexus 128 scanner, Michigan, USA). For *in vitro* PA imaging, the images of CuS NDs and CuS-DDTC NDs solutions with various concentrations were measured. For *in vivo* PA imaging, the CuS NDs and CuS-DDTC NDs solutions (200 μL, 10 mg/kg) were intravenously injected into the 4T1-TBM, respectively, along with the injection of PBS as a control group. After post-injection for various times, PA signals of the tumor site were recorded.

Thermal imaging. The CuS NDs and CuS-DDTC NDs solutions (200 μL, 10 mg/kg) were intravenously injected into the 4T1-TBM, respectively, along with the injection of PBS as a control group. After 12 h of injection, the tumor site was exposed under 808-nm laser (1.5 W/cm^2, 5 min). The temperatures and images were recorded every 1 min using an infrared camera (Tis65, FLUKE, Washington, USA).

Biocompatibility, biodistribution, and metabolism studies. For biocompatibility study, healthy female Kunming (KM, Huafukang Bioscience) mice were used. After intravenous injection with CuS NDs or CuS-DDTC NDs (200 μL, 10 mg/kg) for 14 d, blood was collected for the tests. The major organs, including liver, spleen, lung, kidney, and heart, were collected for Hematoxylin and Eosin (H&E, Keygen) staining, and imaged using a microscope (BX43, Olympus, Tokyo, Japan). For the biodistribution of CuS NDs and CuS-DDTC NDs, 4T1-TBM were used. After intravenous

injection with CuS NDs or CuS-DDTC NDs (200 μL, 10 mg/kg) for various times, the mice were euthanized to collect the tumors and major organs. These collected tissues were weighed and treated with aqua regia. For evaluating Cu metabolism, after intravenous injection for various times, the feces and urine were collected and treated with aqua regia. Finally, the amount of Cu in the major organs, tumors, feces, and urine were analyzed using Inductively Coupled Plasma-Mass Spectrometry (ICP-MS, Agilent 7800, Tokyo, Japan).

Anti-cancer effects. The 4T1-TBM were randomly divided into different groups, including NIR laser (PBS + L), DDTC, CuS NDs, CuS-DDTC NDs, CuS NDs + NIR laser (CuS + L), CuS-DDTC NDs + NIR laser (CuS-DDTC + L), and PBS groups (n = 4). The samples containing CuS NDs or CuS-DDTC NDs were intravenously injected (200 μL, 10 mg/kg) in all corresponding groups, respectively. After 12 h, the PBS + L, CuS + L, and CuS-DDTC + L groups were exposed under the 808-nm laser (1.5 W/cm^2, 5 min). After 14 d of treatment, the mice were euthanized to collect tumors. Finally, the weights of the tumors were recorded.

RESULTS AND DISCUSSION

Synthesis and characterizations. The construction of CuS-DDTC NDs was depicted in **Scheme 1**. First, PVP-coated CuS NDs were fabricated *via* the chemical reaction of S^{2-} and Cu^{2+} ions.[25] As shown in **Figure 1**A, the average diameter of the synthesized CuS NDs was about 8.8 nm, and no significant agglomerations were observed. **Figure 1**B showed that CuS NDs possessed strong NIR absorption in the NIR bio-window (750 – 1100 nm), which could be optimum for PTT, PA, and thermal imaging.[24, 36] Further, the chemical status of CuS NDs was assessed by the X-ray photoelectron spectroscopy (XPS, K-Alpha+, Thermo Fisher Scientific, Waltham, USA), and the Cu and S signals were appeared in the XPS spectrum (**Figure 1**C), which confirmed the formation of CuS NDs. Next, to achieve the complexation between copper and DDTC, DDTC was

added in the CuS NDs solution to prepare CuS-DDTC NDs. The loading capacity under the different mass ratios of CuS NDs to DDTC was measured. In the UV-vis-NIR absorption curve (**Figure 1**D), the characteristic absorption peak at 433 nm could be ascribed to $Cu(DDTC)_2$, indicating that DDTC was successfully loaded on the CuS NDs surface. With increasing the amount of DDTC, the absorbance at 433 nm increased gradually, suggesting that the loading efficiency was enhanced and was up to 19.5 %, while CuS: DDTC was 0.25 (**Figure 1**E). In addition, no apparent morphological change was observed on CuS NDs with the increasing amount of surface DDTC (**Figure S2**). Moreover, the DLS measurements showed that the zeta potential values of both CuS NDs, as well as CuS-DDTC NDs, were in the negative range (**Figure 1**F), but the dispersity decreased slightly (**Figure 1**F). Similarly, the particle size gradually increased with the increasing amount of surface DDTC in **Figure S3**, indicating that the higher DDTC content might have affected the dispersibility of the particles and led to an increase in the hydrodynamic size of CuS NDs. In addition to the drug loading and physicochemical properties of CuS NDs, the biocompatibility of CuS-DDTC NDs was investigated using HUVECs.[21] The experimental results showed that the mass ratio of higher 50:1, CuS-DDTC NDs were highly toxic to HUVECs (**Figure S4**). Therefore, the mass ratio of 100:1, exhibiting excellent dispersibility, and the least toxicity to normal cells, was chosen for the subsequent experiments. After the loading process of DDTC on CuS NDs, the characteristic peaks of DDTC and $Cu(DDTC)_2$ at 280 nm and 433 nm were disappeared entirely in the spectrum of supernatant, respectively, indicating that DDTC was fully loaded on the CuS NDs surface (**Figure 1**H). In addition, the XRD patterns showed that CuS NDs were hexagonal-phase, and the characteristic peak of $Cu(DDTC)_2$ was discovered in CuS-DDTC NDs (**Figure 1**I).[23] These results demonstrated that CuS NDs were well-prepared, DDTC was successfully loaded on the surface of CuS NDs.

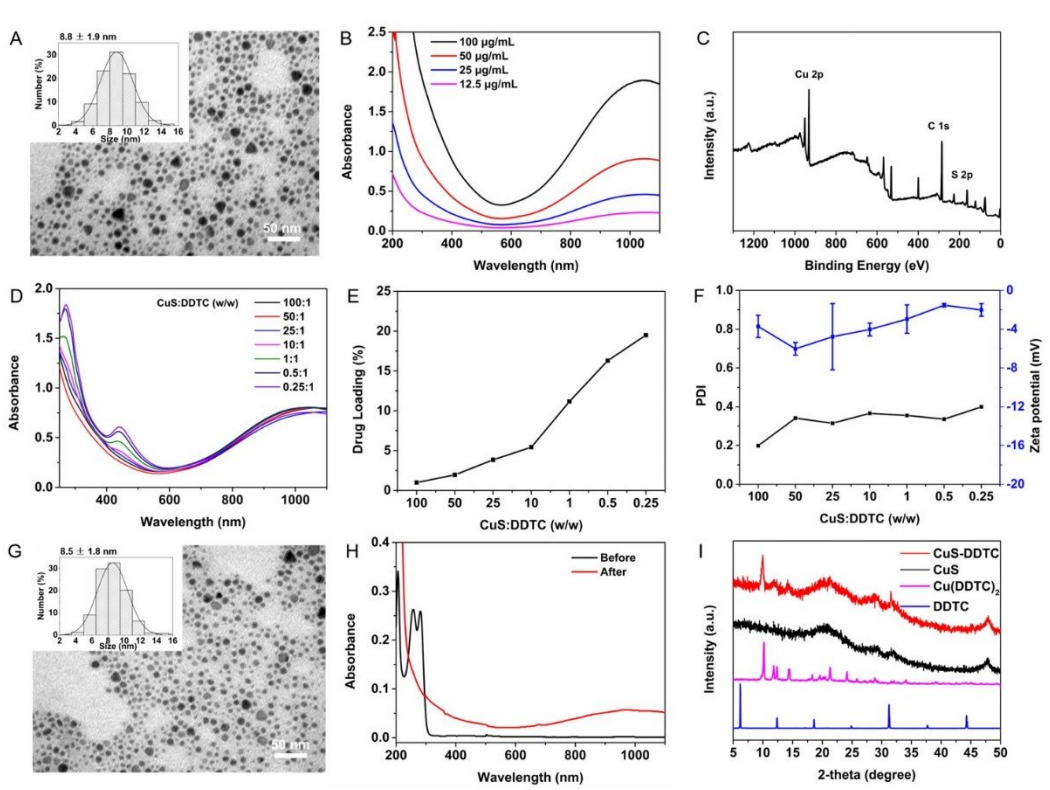

Figure 1. Characterizations of CuS NDs and CuS-DDTC NDs. A. TEM image of CuS NDs and the histogram in the inset showing the size distribution of CuS NDs. B. UV-vis-NIR spectra of the CuS NDs suspension. C. XPS spectrum of CuS NDs. D. UV-vis-NIR spectra of the CuS-DDTC NDs solution with different mass ratios. E. Drug loading efficiency of the CuS-DDTC NDs with different mass ratios. F. Zeta potential, and PDI of the CuS-DDTC NDs solution with different mass ratios. G. TEM image of CuS-DDTC NDs at the mass ratio of 100:1, and the histogram in the inset showing the size distribution. H. UV-vis-NIR spectrum of supernatant before and after drug loading. I. XRD patterns of DDTC, $Cu(DDTC)_2$, CuS NDs, and CuS-DDTC NDs.

Photothermal and photodynamic efficacies *in vitro*. The photothermal properties of CuS NDs were tested using the 808-nm laser. The temperature of the CuS NDs solution (100 μg/mL) irradiated at various power densities (0.5, 1.0, 1.5, and 2.0 W/cm^2, 15 min) was increased to 5.1, 10.2, 13.4, and 19.2 °C, respectively (**Figure 2**A). Further, the photothermal conversion rates of

CuS NDs at various power densities (0.5, 1.0, 1.5, and 2.0 W/cm^2) were calculated by using the previously reported method as 60.9, 61.2, 53.7, and 56.5 %, respectively, suggesting that CuS NDs had shown excellent photothermal conversion performance.[35] In addition, the results of cyclic photothermal experiments of CuS NDs showed that the photothermal conversion ability remained stable (**Figure 2**B), and the UV-vis-NIR absorption spectrum remained unchanged throughout the experiments (**Figure 2**C). The temperature of CuS-DDTC NDs solution (100 μg/mL) raised to 13.4 °C after irradiation (1.5 W/cm^2, 15 min) in **Figure 2**D, demonstrating that the photothermal conversion performance of CuS-DDTC NDs was not affected by DDTC.

To investigate the photodynamic properties of CuS-DDTC NDs, we monitored the generation of •OH and $^1O_2$ radicals by using the formation reaction of 2-hydroxy-terephalic acid (TAOH) and the degradation reaction of the ABMDMA, respectively.[16] **Figure 2**E and **2**F indicated that the fluorescence of TAOH enhanced rapidly at 360 nm, and the absorption of ABMDMA decreased slightly at 380 nm with CuS NDs and CuS-DDTC NDs (**Figure S5**), suggesting the substantial generation of free radicals, •OH, and $^1O_2$ radicals. Moreover, the production rates of ROS without laser irradiation were also higher than that pure TA or ABMDMA irradiated without CuS NDs and CuS-DDTC NDs. These results were agreement with the reported studies,[24] indicating CuS was a good nano-catalyst for Fenton-like reaction. Meanwhile, the reaction rates under laser irradiation were faster than that of without irradiation (**Figure 2**F), which could be due to the leakage of copper ions under laser irradiation. In addition, because of the formation of $Cu(DDTC)_2$, the reaction rate of CuS-DDTC NDs was faster than CuS NDs in **Figure 2**F.[37] All these results demonstrate the potential of CuS-DDTC NDs in PTT and PDT.

To investigate the degradation process of CuS NDs and CuS-DDTC NDs, CuS NDs and CuS-DDTC NDs were incubated in PBS *in vitro*, respectively. The UV-vis-NIR spectrum indicated that

the absorbance of CuS decreased with the increase of incubation time (**Figure 2**G and **2**H), which indicated that CuS NDs and CuS-DDTC NDs could be degraded in physiological buffer.[23] Due to the ease of oxidation and rapid degradation of (102) surface, the copper ions were released from the CuS NDs, which was conducive to the degradation of CuS NDs and the production of ROS, further avoiding the long-term toxicity and favorable for the production of $Cu(DDTC)_2$.

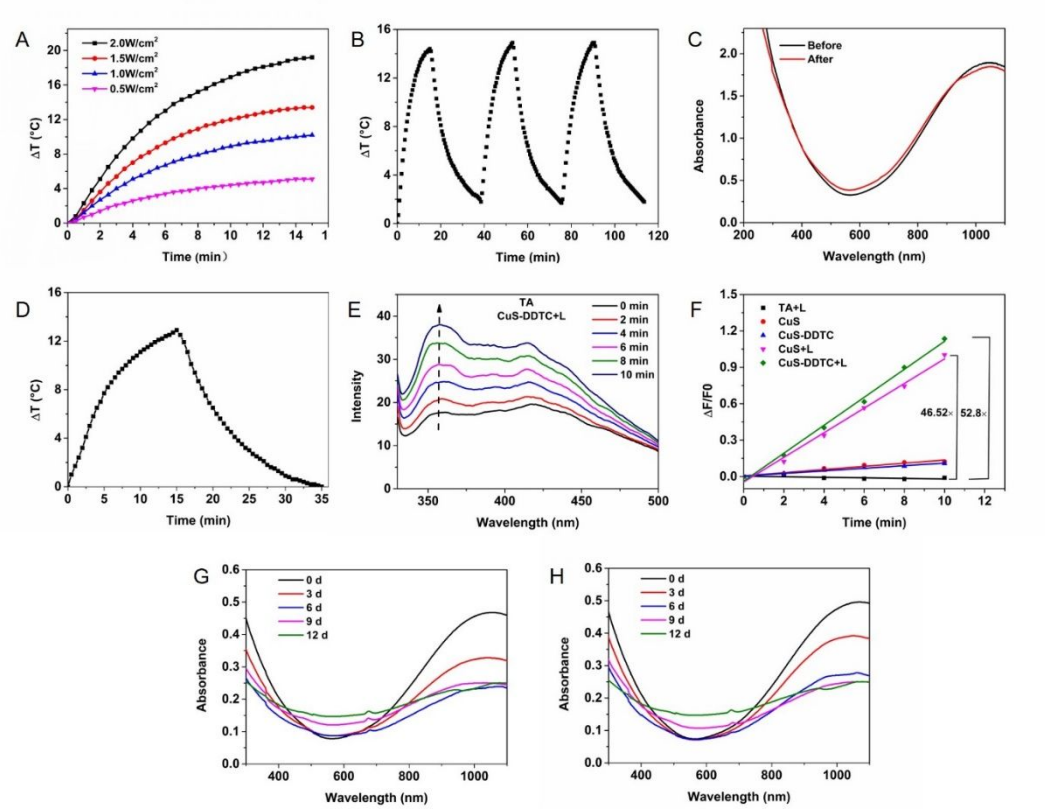

Figure 2. *In vitro* photothermal and photodynamic performances. A. The temperature change curves of CuS NDs solutions under different laser power densities. B. The temperature change curves of CuS NDs solutions with three temperature cycles. C. UV-vis-NIR spectra of the CuS NDs before and after laser irradiation. D. The temperature change curve of CuS-DDTC NDs solutions under 1.5 W/cm^2 laser irradiation. E. The change of the fluorescence spectra of TA solution in the presence of CuS-DDTC NDs under laser irradiation. F. A variation in the

fluorescence intensity of TAOH at 360 nm under different treatment. G. UV-vis-NIR spectra of CuS NDs PBS suspension. H. UV-vis-NIR spectra of CuS-DDTC NDs PBS suspension at different time points.

***In vitro* synergistic therapeutic effects.** Before exploring the synergistic effect of chemo-PTT *in vitro*, we first studied the intracellular uptake efficacy of CuS NDs. In **Figure 3**A, the CuS NDs were internalized efficiently into cells in the proximity of the nucleus. Moreover, the fluorescence intensity was enhanced with the extended culture time, representing the increase of the internalized amount of CuS NDs, which is conducive to the photothermal effect.[38-39] Then, the synergistic effect of chemo-PTT effects of the designed formulation was measured. The experimental results depicted that the viabilities of 4T1 cells remained at high rates after incubation with CuS NDs and free DDTC (**Figure 3B**). Then, the viability of cells treated with CuS-DDTC NDs obviously decreased compared to that of free DDTC and CuS NDs, which could be due to the complexation of copper with DDTC. Notably, the designed CuS NDs could effectively deliver DDTC into cells, and then the copper from degraded CuS would be chelated with DDTC, resulting in the active complex of $Cu(DDTC)_2$. Therefore, CuS-DDTC NDs could perform significantly better anticancer effect than CuS NDs and DDTC. Further, the experimental results showed that under the laser irradiation, CuS NDs and CuS-DDTC NDs could effectively kill the 4T1 cells. At the concentration higher than 30 μg/mL, the anti-tumor effect of the CuS-DDTC + L group was significantly higher than that of CuS + L and CuS-DDTC treatment group. In addition, when the concentration was 50 μg/mL, the cell survival rate was close to zero. On the one hand, depending on the excellent photothermal conversion performance of CuS NDs, the intracellular temperature increased significantly, which resulted in a large number of cell death. On the other hand, the photothermal effect might have promoted the release of free copper ions, which would be chelated

to generate more $Cu(DDTC)_2$, indicating the higher efficiency of combined chemo-PTT treatment (**Figure 3**B).

Further, to investigate the intracellular ROS releasing profiles, DCFH-DA was employed. As shown in **Figure 3**C, weak green fluorescence in CuS and CuS-DDTC group and strong green fluorescence in CuS + L and CuS-DDTC + L treatment groups were observed in 4T1 cells by CLSM, representing the presence of ROS. Contrarily, the control and DDTC treatment groups showed a negligible green fluorescence. These results showed that under the laser irradiation, CuS NDs and CuS-DDTC NDs could effectively produce ROS for PDT treatment. In addition, AO/EB staining was used to visualize living and dead cells, respectively. These results showed that the cells in the control, laser, DDTC, and CuS NDs treatment groups displayed strong green fluorescence, representing the living cells (**Figure 3**D). It was observed that CuS-DDTC NDs, CuS + L, and CuS-DDTC + L treatment groups displayed both red and green fluorescence. In comparison, most 4T1 cells in the CuS-DDTC + L group have shown apoptosis with red fluorescence, demonstrating the high efficiency of synergistic therapeutic effect via the combination of photothermal therapy and copper ions-enhanced chemotherapy.

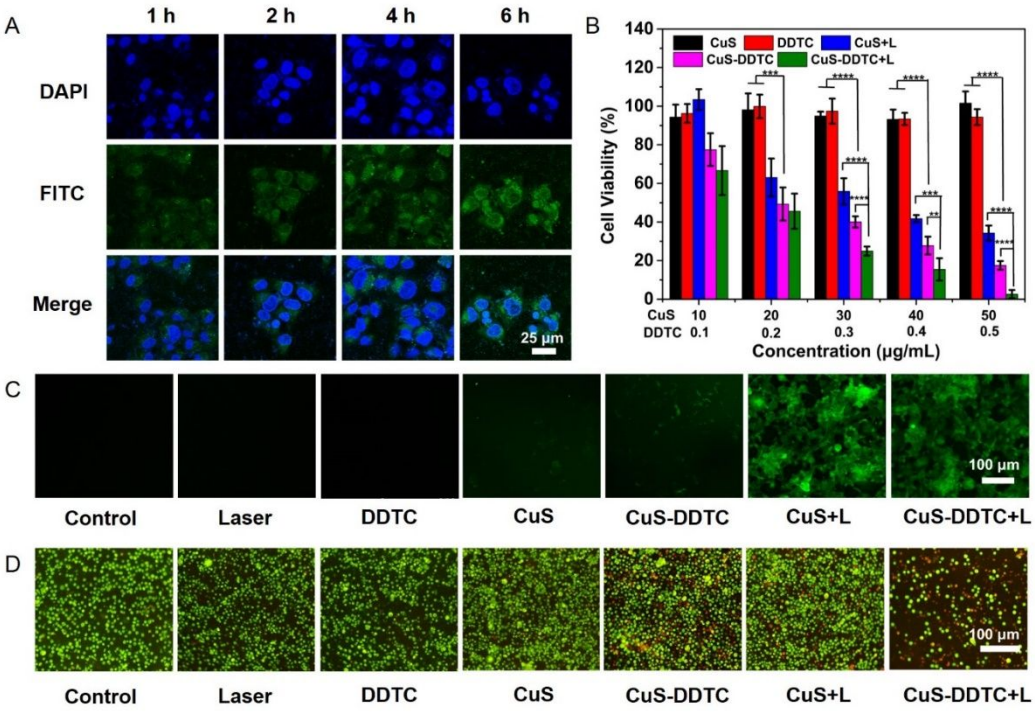

Figure 3. Cellular uptake and synergistic effect of Chemo-PTT *in vitro*. A. Cellular uptake assay of CuS NDs, scale bar is 20 μm. B. Cell viabilities of 4T1 cells. C. DCFH-DA fluorescence images of 4T1 cells, scale bar is 100 μm. D. Live/dead staining images, live cells in green and apoptosis cells in red, scale bar is 100 μm. *** $P < 0.001$ and **** $P < 0.0001$.

Synergistic effect of PTT and copper enhanced chemotherapy *in vivo*. Based on the excellent near-infrared photothermal efficiency, CuS NDs was an ideal PA contrast agent, assisting in the tracking of these composites in the tumor tissue. The PA signals *in vitro* induced by CuS-DDTC NDs and CuS NDs were similar, and both of which increased linearly with the CuS concentrations in **Figure 4**A. Further, we validated their PA imaging efficiency *in vivo*. The 4T1-TBM were injected with CuS NDs and CuS-DDTC NDs, respectively. Then, PA images and signals at various times were recorded (**Figure 4**B and **4**C). The results indicated that with the extended injection time, the PA signal intensity had significantly enhanced and reached a peak at 12 h. Further,

biodistribution and metabolism were investigated using 4T1-TBM to assess the mechanism of the pharmacokinetics of CuS NDs and their efficacy *in vivo*. **Figure 4**D and **4**E showed that CuS-DDTC NDs could be rapidly cleared through feces and urine. After intravenous injection for 48 h, the excretion amounts in feces and urines were nearly 37.2 and 2.8 %, respectively, which was consistent with previous studies.[24] The biodistribution of CuS-DDTC NDs in major organs at different time intervals indicated that the CuS-DDTC NDs were efficiently eliminated (**Figure 4**E). Moreover, after intravenous injection, the designed nanocomposites into 4T1-TBM for 12 h, about 3.0 % of CuS-DDTC NDs were accumulated in the tumor site. Together, our findings demonstrated that CuS-DDTC NDs could be effectively accumulated to tumor site for tumor treatment, and efficiently excreted from the body with low long-term toxicity.

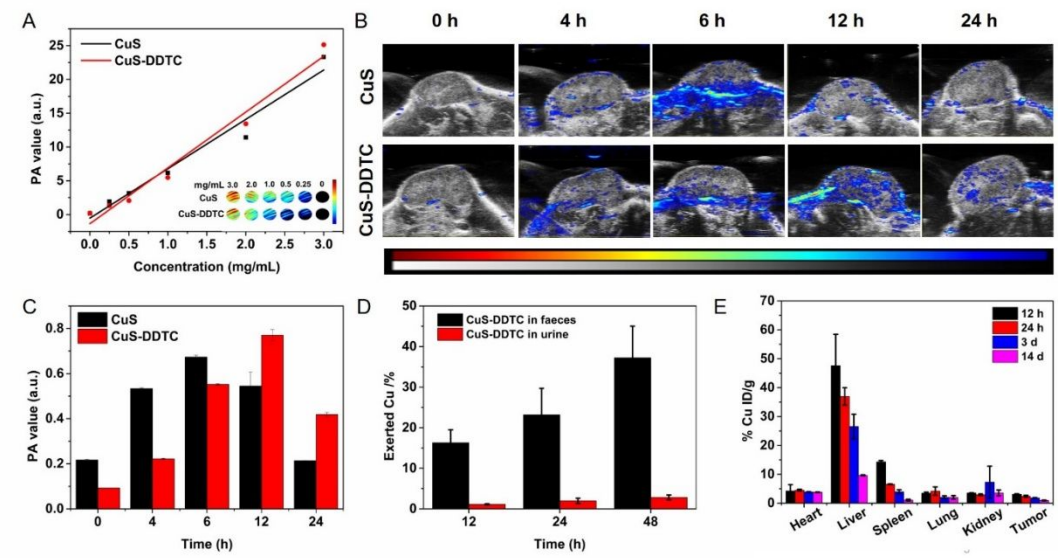

Figure 4. PA imaging and biodistribution of CuS NDs and CuS-DDTC NDs *in vivo*. A. PA images and signal values of CuS NDs and CuS-DDTC NDs solutions with various concentrations. B. PA imaging of 4T1-TBM at various time points. C. PA signal values of CuS NDs and CuS-DDTC NDs *in vivo*. D. Cu excretion in feces and urine. E. Biodistribution of Cu in tumor and main organs.

Next, the biocompatibility *in vivo* was accessed by intravenous injection of CuS NDs and CuS-DDTC NDs into KM healthy mice, respectively, along with PBS as a negative control treatment. After 14 d of intravenous injection, these mice were sacrificed for blood test together with liver and kidney function evaluation. The blood test results in **Figure S8** indicated that there was no obvious difference between the CuS NDs, CuS-DDTC NDs, and PBS treatment groups. These blood test results suggested that CuS NDs and CuS-DDTC NDs had no apparent toxicities. No prominent toxicities and damage in organs were observed after the treatment with CuS NDs and CuS-DDTC NDs (**Figure S9**). All these results indicated that CuS-DDTC NDs were safe for tumor treatment.

Finally, the combined therapeutic efficiency was assessed using 4T1-TBM. Based on the results of PA images and distribution in the tumor site, thermal imaging was performed after intravenously injected with CuS NDs and CuS-DDTC NDs for 12 h. PTT is a highly selective and low toxic treatment method. Accordingly, the tumor tissue can be selectively irradiated with laser light towards precise ablation without causing any damage to normal tissue.[40] In **Figure 5**A and **5**B, the temperature at the tumor site in CuS NDs and CuS-DDTC NDs groups increased about 14 °C and reached to 48 °C, higher than PBS + L group, *i.e.,* 39 °C, suggesting that CuS NDs and CuS-DDTC NDs were the effective photothermal agents for tumor treatment *in vivo*. The CuS NDs or CuS-DDTC NDs were intravenously injected in all corresponding groups, respectively. After 12 h, the PBS + L, CuS + L, and CuS-DDTC + L groups were exposed under the laser (1.5 W/cm^2, 5 min). In **Figure 5**C, no noticeable body-weight loss of mice was observed throughout the treatment period. As demonstrated in **Figure 5**D-F, the tumor volume of PBS, PBS + L, DDTC, and CuS NDs treatment groups increased rapidly, while a particular tumor inhibition effect was observed in the CuS-DDTC group within 4 d after injection. Notably, the tumor growth trend was slowed

down in the CuS-DDTC group. However, CuS-DDTC NDs could be rapidly eliminated by metabolism, and only one injection could not effectively control the tumor growth. In the later stage, tumor cells were grown rapidly, and there was no significant difference in tumor volume between CuS-DDTC and PBS group. Further, compared to the PBS group, CuS + L and CuS-DDTC + L groups showed a remarkable inhibitory effect on tumor growth. In addition, the digital photos of 4T1-TBM (**Figure 5**E) showed that the center part of the tumor in the CuS +L group was eliminated and crusted. However, the edge of the tumor continued to grow to the periphery due to tumor recurrence. As the eliminated part of the tumor was calculated in the tumor volume, but not included in the tumor weight, the tumor weight results (**Figure 5**F) showed that there had a significant difference between PBS, CuS + L, and CuS-DDTC + L groups. The growth of tumors was inhibited in the CuS-DDTC + L group without reoccurrence in the 14 d of the treatment (**Figure 5**D-F), while contrarily, the tumors in CuS + L group were relapsed in 8 d of the treatment. The substantial tumor inhibition effects of the CuS-DDTC + L group over the CuS + L treatment group could be due to combined copper-dependent chemo-phototherapy therapy. In addition, the blood samples were collected for the blood tests after 14 d of treatment. The experimental results showed that only the blood indices of CuS-DDTC + L group were within the normal range, demonstrating the mice were healthy and the tumors were eliminated without reoccurrence in the CuS-DDTC + L group (**Figure S10**). These *in vivo* results indicated the CuS-DDTC NDs were promising for cancer treatment applications with high biosafety.

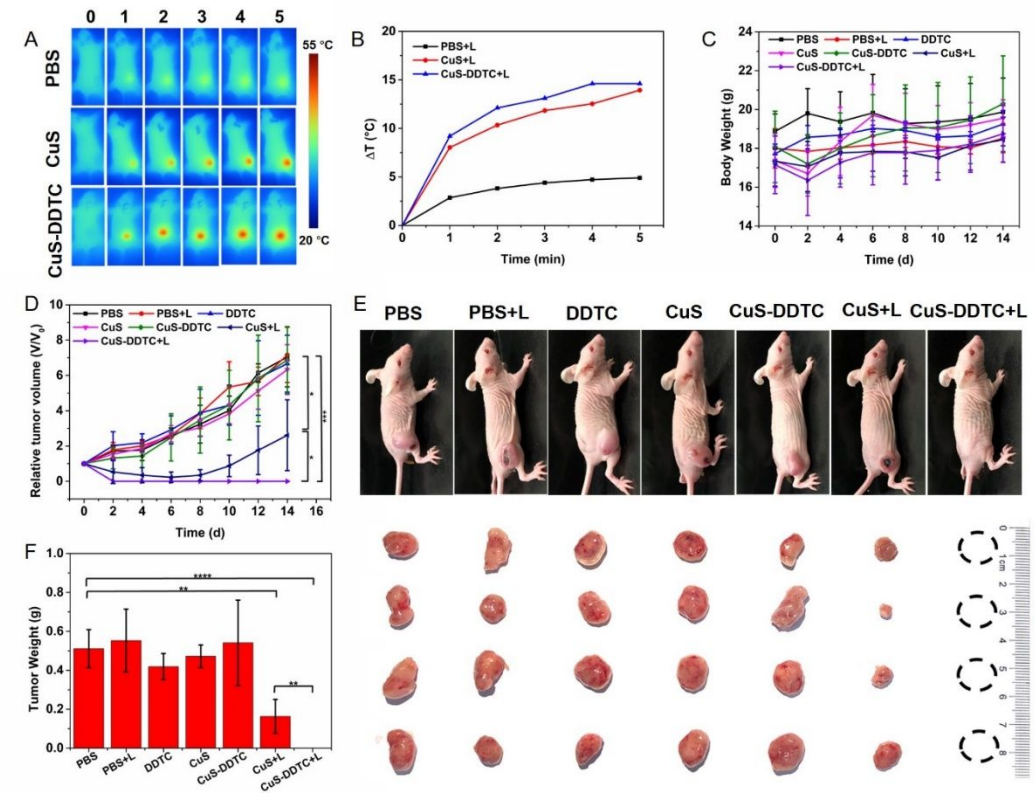

Figure 5. Synergistic therapy *in vivo*. A. Thermal imaging of 4T1-TBM injected with PBS, CuS NDs, and CuS-DDTC NDs under the laser irradiation (1.5 W/cm^2, 5 min) post intravenous injection for 12 h. B. The temperature change at the tumor site. C. Body weight of 4T1-TBM with different treatments. D. Tumor volume change curves. E. Digital photos of 4T1-TBM and tumors after different treatments for 14 d. F. Tumor weights after different treatments for 14 d. * $P < 0.05$, ** $P < 0.01$, *** $P < 0.001$, and **** $P < 0.0001$.

CONCLUSION

In conclusion, we have successfully fabricated a biodegradable multi-functional nanoplatform based on CuS-DDTC NDs possessing capabilities of multimodal imaging along with the synergistic effect of combined photothermal and copper ions-enhanced chemotherapy. As a DDS and copper source, CuS NDs could effectively deliver DDTC and copper ions to the tumor sites. Due to the degradation and photothermal effect of CuS NDs, copper ions were released and

chelated with DDTC to generate $Cu(DDTC)_2$ and improve the anti-tumor effect. Because of the synergistic therapeutic effect, CuS-DDTC NDs exhibited an excellent anti-tumor effect *in vivo*. Therefore, CuS-DDTC NDs could efficiently inhibit tumor growth and be readily degraded as well as excreted *in vivo* without showing long-term toxicity. These results indicated that CuS-DDTC NDs have huge potential for cancer treatment in future clinical applications.

ASSOCIATED CONTENT

Supporting Information.

Supplementary information includes UV–vis, TEM, DLS, cell viabilities, H&E staining, and hematology data.

AUTHOR INFORMATION

Corresponding Author

*Ai-Zheng Chen - Email: azchen@hqu.edu.cn

Notes

The authors declare no competing financial interest.

ACKNOWLEDGMENT

We sincerely thank Prof. Gang Liu and Mr. Yang Zhang of Xiamen University, Xiamen, China, for assistance in the photoacoustic imaging experiment. This work was supported by the National

Natural Science Foundation of China (NSFC, 81971734, U1605225, and 31800794) and the Program for Innovative Research Team in Science and Technology in Fujian Province University.

REFERENCES

(1) Liu, F.; Lin, L.; Zhang, Y.; Sheng, S.; Wang, Y.; Xu, C.; Tian, H.; Chen, X. Two-Dimensional Nanosheets with High Curcumin Loading Content for Multimodal Imaging-Guided Combined Chemo-Photothermal Therapy. *Biomaterials* **2019,** *223*, 119470.
(2) Lin, X.; Fang, Y.; Tao, Z.; Gao, X.; Wang, T.; Zhao, M.; Wang, S.; Liu, Y. Tumor-Microenvironment-Induced All-in-One Nanoplatform for Multimodal Imaging-Guided Chemical and Photothermal Therapy of Cancer. *ACS Appl. Mater. Interfaces* **2019,** *11* (28), 25043-25053.
(3) Li, J.; Jiang, R.; Wang, Q.; Li, X.; Hu, X.; Yuan, Y.; Lu, X.; Wang, W.; Huang, W.; Fan, Q. Semiconducting Polymer Nanotheranostics for NIR-II/Photoacoustic Imaging-Guided Photothermal Initiated Nitric Oxide/Photothermal Therapy. *Biomaterials* **2019,** *217*, 119304.
(4) Wang, Z.; Yu, N.; Li, X.; Yu, W.; Han, S.; Ren, X.; Yin, S.; Li, M.; Chen, Z. Galvanic Exchange-Induced Growth of Au Nanocrystals on CuS Nanoplates for Imaging Guided Photothermal Ablation of Tumors. *Chem. Eng. J.* **2020,** *381*, 122613.
(5) Chen, B. Q.; Kankala, R. K.; Zhang, Y.; Xiang, S. T.; Tang, H. X.; Wang, Q.; Yang, D. Y.; Wang, S. B.; Zhang, Y. S.; Liu, G.; Chen, A. Z. Gambogic Acid Augments Black Phosphorus Quantum Dots (BPQDs)-Based Synergistic Chemo-Photothermal Therapy through Downregulating Heat Shock Protein Expression. *Chem. Eng. J.* **2020,** *390*, 124312.
(6) Zhang, H.; Chen, Y.; Cai, Y.; Liu, J.; Liu, P.; Li, Z.; An, T.; Yang, X.; Liang, C. Paramagnetic CuS Hollow Nanoflowers for T2-FLAIR Magnetic Resonance Imaging-Guided Thermochemotherapy of Cancer. *Biomater. Sci.* **2019,** *7* (1), 409-418.
(7) Jia, Y.; Song, Y.; Qu, Y.; Peng, J.; Shi, K.; Du, D.; Li, H.; Lin, Y.; Qian, Z. Mesoporous PtPd Nanoparticles for Ligand-Mediated and Imaging-Guided Chemo-Photothermal Therapy of Breast Cancer. *Nano Res.* **2020,** *13* (6), 1739-1748.
(8) Shi, Z.; Zhou, Y.; Fan, T.; Lin, Y.; Zhang, H.; Mei, L. Inorganic Nano-Carriers Based Smart Drug Delivery Systems for Tumor Therapy. *Smart Mater. Med.* **2020,** *1*, 32-47.
(9) Liu, C. G.; Han, Y. H.; Zhang, J. T.; Kankala, R. K.; Wang, S. B.; Chen, A. Z. Rerouting Engineered Metal-Dependent Shapes of Mesoporous Silica Nanocontainers to Biodegradable Janus-Type (Sphero-Ellipsoid) Nanoreactors for Chemodynamic Therapy. *Chem. Eng. J.* **2019,** *370*, 1188-1199.
(10) Wang, Y.; Liu, X.; Deng, G.; Sun, J.; Yuan, H.; Li, Q.; Wang, Q.; Lu, J. Se@ SiO_2–FA–CuS Nanocomposites for Targeted Delivery of DOX and Nano Selenium in Synergistic Combination of Chemo-Photothermal Therapy. *Nanoscale* **2018,** *10* (6), 2866-2875.
(11) Lu, N.; Fan, W.; Yi, X.; Wang, S.; Wang, Z.; Tian, R.; Jacobson, O.; Liu, Y.; Yung, B. C.; Zhang, G. Biodegradable Hollow Mesoporous Organosilica Nanotheranostics for Mild Hyperthermia-Induced Bubble-Enhanced Oxygen-Sensitized Radiotherapy. *ACS Nano* **2018,** *12* (2), 1580-1591.
(12) Li, Q. L.; Wang, D.; Cui, Y.; Fan, Z.; Ren, L.; Li, D.; Yu, J. AIEgen-Functionalized Mesoporous Silica Gated by Cyclodextrin-Modified CuS for Cell Imaging and Chemo-

Photothermal Cancer Therapy. *ACS Appl. Mater. Interfaces* **2017,** *10* (15), 12155-12163.
(13) Goel, S.; Ferreira, C. A.; Chen, F.; Ellison, P. A.; Siamof, C. M.; Barnhart, T. E.; Cai, W. Activatable Hybrid Nanotheranostics for Tetramodal Imaging and Synergistic Photothermal/Photodynamic Therapy. *Adv. Mater.* **2018,** *30* (6), 1704367.
(14) Wang, X.; Cui, X.; Zhao, Y.; Chen, C. Nano-Bio Interactions: the Implication of Size-Dependent Biological Effects of Nanomaterials. *Sci. China Life Sci.* **2020,** *63*, 1168-1182.
(15) Mao, F.; Liu, Y.; Ma, L.; Liu, L.; Jiang, A.; Zhai, X.; Zhou, J. Green Synthesis of Ultra-Small VOx Nanodots for Acidic-Activated HSP60 Inhibition and Therapeutic Enhancement. *Biomaterials* **2019,** *194*, 94-104.
(16) Zhang, H.; Wang, T.; Liu, H.; Ren, F.; Qiu, W.; Sun, Q.; Yan, F.; Zheng, H.; Li, Z.; Gao, M. Second Near-Infrared Photodynamic Therapy and Chemotherapy of Orthotopic Malignant Glioblastoma with Ultra-small $Cu_{2-X}Se$ Nanoparticles. *Nanoscale* **2019,** *11* (16), 7600-7608.
(17) Zhang, A.; Li, A.; Zhao, W.; Yan, G.; Liu, B.; Liu, M.; Li, M.; Huo, B.; Liu, J. An Efficient and Self-Guided Chemo-Photothermal Drug Loading System Based on Copolymer and Transferrin Decorated MoS_2 Nanodots for Dually Controlled Drug Release. *Chem. Eng. J.* **2018,** *342*, 120-132.
(18) Wang, R.; He, Z.; Cai, P.; Zhao, Y.; Gao, L.; Yang, W.; Zhao, Y.; Gao, X.; Gao, F. Surface-Functionalized Modified Copper Sulfide Nanoparticles Enhance Checkpoint Blockade Tumor Immunotherapy by Photothermal Therapy and Antigen Capturing. *ACS Appl. Mater. Interfaces* **2019,** *11* (15), 13964-13972.
(19) Dang, Y.; Guan, J. Nanoparticle-Based Drug Delivery Systems for Cancer Therapy. *Smart Mater. Med.* **2020,** *1*, 10-19.
(20) Feng, Q.; Zhang, W.; Li, Y.; Yang, X.; Hao, Y.; Zhang, H.; Li, W.; Hou, L.; Zhang, Z. An Intelligent NIR-Responsive Chelate Copper-Based Anticancer Nanoplatform for Synergistic Tumor Targeted Chemo-Phototherapy. *Nanoscale* **2017,** *9* (40), 15685-15695.
(21) Wu, W.; Yu, L.; Pu, Y.; Yao, H.; Chen, Y.; Shi, J. Copper - Enriched Prussian Blue Nanomedicine for In Situ Disulfiram Toxification and Photothermal Antitumor Amplification. *Adv. Mater.* **2020,** *32* (17), 2000542.
(22) Kankala, R. K.; Liu, C. G.; Yang, D. Y.; Wang, S. B.; Chen, A. Z. Ultrasmall Platinum Nanoparticles Enable Deep Tumor Penetration and Synergistic Therapeutic Abilities through Free Radical Species-Assisted Catalysis to Combat Cancer Multidrug Resistance. *Chem. Eng. J.* **2020,** *383*, 123138.
(23) Dong, L.; Li, K.; Wen, D.; Lu, Y.; Du, K.; Zhang, M.; Gao, X.; Feng, J.; Zhang, H. A Highly Active (102) Surface-Induced Rapid Degradation of A CuS Nanotheranostic Platform for In Situ T1-Weighted Magnetic Resonance Imaging-Guided Synergistic Therapy. *Nanoscale* **2019,** *11* (27), 12853-12857.
(24) Hu, R.; Fang, Y.; Huo, M.; Yao, H.; Wang, C.; Chen, Y.; Wu, R. Ultrasmall $Cu_{2-X}S$ Nanodots As Photothermal-Enhanced Fenton Nanocatalysts for Synergistic Tumor Therapy at NIR-II Biowindow. *Biomaterials* **2019,** *206*, 101-114.
(25) Zhou, M.; Li, J.; Liang, S.; Sood, A. K.; Liang, D.; Li, C. CuS Nanodots with Ultrahigh Efficient Renal Clearance for Positron Emission Tomography Imaging and Image-Guided Photothermal Therapy. *ACS Nano* **2015,** *9* (7), 7085-7096.
(26) Skrott, Z.; Mistrik, M.; Andersen, K. K.; Friis, S.; Majera, D.; Gursky, J.; Ozdian, T.; Bartkova, J.; Turi, Z.; Moudry, P. Alcohol-Abuse Drug Disulfiram Targets Cancer via p97 Segregase Adaptor NPL4. *Nature* **2017,** *552* (7684), 194-199.
(27) Wang, S.; Riedinger, A.; Li, H.; Fu, C.; Liu, H.; Li, L.; Liu, T.; Tan, L.; Barthel, M. J.; Pugliese,

G. Plasmonic Copper Sulfide Nanocrystals Exhibiting Near-Infrared Photothermal and Photodynamic Therapeutic Effects. *ACS Nano* **2015,** *9* (2), 1788-1800.
(28) Ku, G.; Zhou, M.; Song, S.; Huang, Q.; Hazle, J.; Li, C. Copper Sulfide Nanoparticles As A New Class of Photoacoustic Contrast Agent for Deep Tissue Imaging at 1064 nm. *ACS Nano* **2012,** *6* (8), 7489-7496.
(29) Mou, J.; Li, P.; Liu, C.; Xu, H.; Song, L.; Wang, J.; Zhang, K.; Chen, Y.; Shi, J.; Chen, H. Ultrasmall $Cu_{2-X}S$ Nanodots for Highly Efficient Photoacoustic Imaging‐Guided Photothermal Therapy. *Small* **2015,** *11* (19), 2275-2283.
(30) Iljin, K.; Ketola, K.; Vainio, P.; Halonen, P.; Kohonen, P.; Fey, V.; Grafström, R. C.; Perälä, M.; Kallioniemi, O. High-Throughput Cell-Based Screening of 4910 Known Drugs and Drug-Like Small Molecules Identifies Disulfiram As An Inhibitor of Prostate Cancer Cell Growth. *Clin. Cancer Res.* **2009,** *15* (19), 6070-6078.
(31) Chen, D.; Cui, Q. C.; Yang, H.; Dou, Q. P. Disulfiram, A Clinically Used Anti-Alcoholism Drug and Copper-Binding Agent, Induces Apoptotic Cell Death in Breast Cancer Cultures and Xenografts via Inhibition of the Proteasome Activity. *Cancer Res.* **2006,** *66* (21), 10425-10433.
(32) Bakthavatsalam, S.; Sleeper, M. L.; Dharani, A.; George, D. J.; Zhang, T.; Franz, K. J. Leveraging γ-Glutamyl Transferase To Direct Cytotoxicity of Copper Dithiocarbamates against Prostate Cancer Cells. *Angew. Chem. Int. Ed.* **2018,** *57* (39), 12780-12784.
(33) He, H.; Markoutsa, E.; Li, J.; Xu, P. Repurposing Disulfiram for Cancer Therapy via Targeted Nanotechnology through Enhanced Tumor Mass Penetration and Disassembly. *Acta Biomater.* **2018,** *68*, 113-124.
(34) Pan, Q.; Zhang, B.; Peng, X.; Wan, S.; Luo, K.; Gao, W.; Pu, Y.; He, B. A Dithiocarbamate-Based H_2O_2-Responsive Prodrug for Combinational Chemotherapy and Oxidative Stress Amplification Therapy. *Chem. Commun.* **2019,** *55* (92), 13896-13899.
(35) Ren, W.; Yan, Y.; Zeng, L.; Shi, Z.; Gong, A.; Schaaf, P.; Wang, D.; Zhao, J.; Zou, B.; Yu, H. A Near Infrared Light Triggered Hydrogenated Black TiO_2 for Cancer Photothermal Therapy. *Adv. healthcare Mater.* **2015,** *4* (10), 1526-1536.
(36) Zhang, H.; Zeng, W.; Pan, C.; Feng, L.; Ou, M.; Zeng, X.; Liang, X.; Wu, M.; Ji, X.; Mei, L. SnTe@MnO_2-SP Nanosheet–Based Intelligent Nanoplatform for Second Near-Infrared Light–Mediated Cancer Theranostics. *Adv. Funct. Mater.* **2019,** *29* (37), 1903791.
(37) Wu, W.; Yu, L.; Jiang, Q.; Huo, M.; Lin, H.; Wang, L.; Chen, Y.; Shi, J. Enhanced Tumor-Specific Disulfiram Chemotherapy by In Situ Cu^{2+} Chelation-Initiated Nontoxicity-to-Toxicity Transition. *J. Am. Chem. Soc.* **2019,** *141* (29), 11531-11539.
(38) Cao, Y.; Wu, T.; Zhang, K.; Meng, X.; Dai, W.; Wang, D.; Dong, H.; Zhang, X. Engineered Exosome-Mediated Near-Infrared-II Region V_2C Quantum Dot Delivery for Nucleus-Target Low-Temperature Photothermal Therapy. *ACS Nano* **2019,** *13* (2), 1499-1510.
(39) Zeng, X.; Yan, S.; Chen, P.; Du, W.; Liu, B. F. Modulation of Tumor Microenvironment by Metal-Organic-Framework-Derived Nanoenzyme for Enhancing Nucleus-Targeted Photodynamic Therapy. *Nano Res.* **2020,** *13* (6), 1527-1535.
(40) Xu, Y.; Li, H.; Fan, L.; Chen, Y.; Li, L.; Zhou, X.; Li, R.; Cheng, Y.; Chen, H.; Yuan, Z. Development of Photosensitizer-Loaded Lipid Droplets for Photothermal Therapy Based on Thiophene Analogs. *J. Adv. Res.* **2020**.

Table of Contents